Analysis of whispering-gallery microcavity-enhanced chemical absorption sensors

A. T. Rosenberger

Department of Physics, Oklahoma State University, Stillwater, OK 74078-3072, USA
atr@okstate.edu

Abstract: A theoretical analysis of the operation of a chemical sensor based on cavity-enhanced optical absorption is given for a system in which the cavity is a dielectric whispering-gallery microresonator. Continuous-wave input is assumed, and the detection sensitivity is characterized in terms of an effective absorption path length. In the case of tunable single-frequency input, it is shown that monitoring analyte-induced changes in the throughput dip depth enables detection with relative sensitivity greater than that of frequency-shift and cavity-ringdown methods. In addition, for the case of broadband input and drop-port output, an analysis applicable to microcavity-enhanced absorbance spectroscopy experiments is given.

OCIS codes: (350.3950) Micro-optics; (300.1030) Absorption; (230.5750) Resonators; (060.2370) Fiber optics sensors.

References and links

1. A. B. Matsko and V. S. Ilchenko, "Optical Resonators with Whispering-Gallery Modes – Part I: Basics," IEEE J. Sel. Top. Quantum Electron. **12**, 3-14 (2006).
2. V. S. Ilchenko and A. B. Matsko, "Optical Resonators with Whispering-Gallery Modes – Part II: Applications," IEEE J. Sel. Top. Quantum Electron. **12**, 15-32 (2006).
3. I. Teraoka, S. Arnold, and F. Vollmer, "Perturbation approach to resonance shifts of whispering-gallery modes in a dielectric microsphere as a probe of a surrounding medium," J. Opt. Soc. Am. B **20**, 1937-1946 (2003).
4. N. M. Hanumegowda, C. J. Stica, B. C. Patel, I. White and X. Fan, "Refractometric sensors based on microsphere resonators," Appl. Phys. Lett. **87**, 201107 (2005).
5. A. M. Armani and K. J. Vahala, "Heavy water detection using ultra-high-*Q* microcavities," Opt. Lett. **31**, 1896-1898 (2006).
6. A. A. Savchenkov, A. B. Matsko, M. Mohageg, and L. Maleki, "Ringdown spectroscopy of stimulated Raman scattering in a whispering gallery mode resonator," Opt. Lett. **32**, 497-499 (2007).
7. R. W. Boyd and J. E. Heebner, "Sensitive disk resonator photonic biosensor," Appl. Opt. **40**, 5742-5747 (2001).
8. M. J. Humphrey, E. Dale, A. T. Rosenberger, and D. K. Bandy, "Calculation of optimal fiber radius and whispering-gallery mode spectra for a fiber-coupled microsphere," Opt. Commun. **271**, 124-131 (2007).
9. M. L. Gorodetsky and V. S. Ilchenko, "Optical microsphere resonators: optimal coupling to high-*Q* whispering-gallery modes," J. Opt. Soc. Am. B **16**, 147-154 (1999).
10. M. Cai, O. Painter, and K. J. Vahala, "Observation of Critical Coupling in a Fiber Taper to a Silica-Microsphere Whispering-Gallery Mode System," Phys. Rev. Lett. **85**, 74-77 (2000).
11. G. Farca, S. I. Shopova, and A. T. Rosenberger are preparing a manuscript to be called "Cavity-enhanced laser absorption spectroscopy using microresonator whispering-gallery modes."
12. M. L. Gorodetsky and V. S. Ilchenko, "High-Q optical whispering-gallery microresonators: precession approach for spherical mode analysis and emission patterns with prism couplers," Opt. Commun. **113**, 133-143 (1994).
13. J. Zhang, B. N. Strecker, R. K. Shelton, S.-J. Ja, J. V. Hryniewicz, and A. T. Rosenberger are preparing a manuscript to be called "A broadband whispering-gallery mode microsphere absorbance spectrometer."
14. S. L. Westcott, J. Zhang, R. K. Shelton, N. M. K. Bruce, S. Gupta, S. L. Keen, J. W. Tillman, L. B. Wald, B. N. Strecker, A. T. Rosenberger, R. R. Davidson, W. Chen, K. G. Donovan, and J. V. Hryniewicz are preparing a manuscript to be called "Broadband optical absorbance spectroscopy using a whispering gallery mode microsphere resonator."

#86369 - $15.00 USD Received 13 Aug 2007; revised 15 Sep 2007; accepted 17 Sep 2007; published 24 Sep 2007

1. Introduction

Dielectric microresonators that support whispering-gallery modes (WGMs) are becoming increasingly useful for numerous applications in optics. These resonators can be spherical, cylindrical, disk-shaped, or toroidal; light in a WGM circulates around the circumference of the resonator, localized near the surface by total internal reflection. The impact of these devices is based on certain attractive properties of WGMs, such as high quality factor (Q) and low mode volume, and on the possibility of efficient coupling of light into and out of these modes [1]. The high Q of a WGM means that light makes many round trips in the resonator. This feature, combined with small mode volume and efficient coupling using prisms, angle-polished fibers, or tapered fibers, makes high intracavity power enhancement easy to achieve. Various applications such as filtering, lasing, modulation, nonlinear optics, sensing, and spectroscopy are enabled by these properties of WGMs [2].

In the application area of label-free chemical detection and spectroscopy, several methods of using WGM microresonators have been reported. Part of the WGM field extends outside the dielectric, and it is this evanescent portion that interacts with the surrounding medium. Analyte molecules in the ambient or on the resonator's surface can then be detected by measuring the frequency shift of a WGM caused by the analyte's perturbation of the ambient's index of refraction [3,4]. In addition, analyte absorption will change the effective Q of the WGM, and the modification of mode linewidth can be measured [5]. One can also envision using cavity-ringdown spectroscopy [6]. The method described in this paper is more closely related to other earlier work [7] in that what is measured is the analyte absorption effect, for continuous-wave input, on either the depth of the throughput dip (Section 2) or the strength of the drop signal (Section 3). As explained below, the former can be more sensitive than other tunable single-frequency methods, and the latter lends itself well to broadband spectroscopy. These techniques will be described in the next two sections and discussed further in Section 4.

2. Tunable single-frequency operation

Consider a microcavity in which light is coupled into a WGM from an adiabatically tapered fiber tangentially in contact with the resonator. Tunable single-frequency light is injected at one end of the tapered fiber and the throughput spectrum that is detected at the other end will display a Lorentzian dip for each WGM resonance excited.

The microcavity can be modeled as a four-mirror ring cavity, as depicted in Fig. 1, in which one of the mirrors is partially transmitting while all the others are assumed to be perfect reflectors. The ring cavity model is a valid analog to a fiber-coupled microresonator when only a single fiber mode is excited. For light incident on a microresonator this is accomplished by making the first fiber taper transition adiabatic. However, light coupling out of the microresonator can couple into many fiber modes, and any light coupled into higher-order modes will be lost if the second taper transition is also adiabatic. Fortunately, it is possible to make this lossy coupling into higher-order fiber modes negligibly small by properly choosing the diameter of the tapered fiber [8].

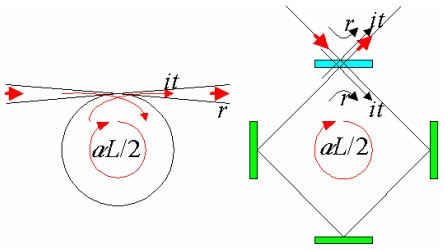

Fig. 1. Four-mirror ring cavity model. Left, microcavity and tapered fiber in contact. Light can couple from the fiber into the resonator and vice versa. Right, the four-mirror ring cavity equivalent. The top mirror is partially transmitting; all others have 100% reflectivity.

#86369 - $15.00 USD Received 13 Aug 2007; revised 15 Sep 2007; accepted 17 Sep 2007; published 24 Sep 2007

A round-trip power loss αL, where α is the loss coefficient and L is the microresonator circumference, is assumed; it models the intrinsic loss (primarily surface scattering) of a WGM microresonator. The mirror reflection and transmission coefficients r and it, relating to the field mode amplitudes, are taken to be real and imaginary respectively without loss of generality; this corresponds to the usual choice for fiber or prism coupling [7,9,10]. The assumption of negligible power loss into radiation modes requires that these coefficients satisfy the relation $t^2 = 1 - r^2$. Because Q is so high, even under conditions of loading by the coupler, the intrinsic round-trip loss and the coupling loss (mirror transmissivity or probability of photon tunneling between fiber and microresonator) will always be small, so $\alpha L << 1$ and $T = t^2 << 1$ will be assumed throughout this work.

By summing the field over round trips, the net reflected power fraction (fiber throughput fraction) is found to be

$$R_\delta = \left| \frac{r - e^{-\alpha L/2} e^{i\delta}}{1 - r e^{-\alpha L/2} e^{i\delta}} \right|^2 , \tag{1}$$

where $\delta = 2\pi n L(\nu - \nu_0)/c$ is the round-trip phase accumulation due to detuning of the input frequency ν from resonance ν_0 (c is the speed of light and n the resonator's index of refraction). The deviation of the throughput fraction from unity gives the dip profile:

$$M_\delta = 1 - R_\delta = \frac{T\alpha L}{\frac{1}{4}(T + \alpha L)^2 + 4\sin^2 \frac{1}{2}\delta} \cong \frac{T\alpha L}{\frac{1}{4}(T + \alpha L)^2 + \delta^2} . \tag{2}$$

This function is the usual Airy profile, with maxima at $\delta = p2\pi$, p = 0, 1, 2, …. The spacing of 2π between adjacent modes is the free spectral range (FSR) in phase. (Recall that the FSR in frequency is given to good approximation by $c/(nL)$. Because many higher-order WGMs can be excited, the actual spacing between adjacent modes is much less than the FSR.) The full width at half-maximum of a WGM resonance is thus seen to be given by $\Delta\delta = T + \alpha L$, the total round-trip loss. The final expression in Eq. (2), valid when $\delta << 1$, shows the Lorentzian profile of a dip.

The dip depth on resonance $(\delta = 0)$ is determined by the ratio of the coupling loss to intrinsic loss, $x = T/\alpha L$, and is given by

$$M_0 = \frac{4x}{(1 + x)^2} . \tag{3}$$

If x = 1, critical coupling is obtained and the dip depth attains its maximum value of 100%; the microresonator is said to be undercoupled if $x < 1$ and overcoupled for $x > 1$. While the coupling loss remains constant, the effective intrinsic loss can be changed by interaction of the evanescent fraction (f) of the WGM with the surrounding medium. The effective loss coefficient can then be written as $\alpha = \alpha_i + f\alpha_a + f\alpha_s$, where the three terms denote true intrinsic loss, absorption (and perhaps also scattering) by the analyte, and absorption in the solvent (or ambient).

Absorption by the analyte causes a change in dip depth that, when small (weak analyte absorption), is proportional to the change in analyte absorption coefficient, in analogy with Beer's law. A theoretical effective absorption path length L_{eff}^t can then be obtained from the dip depth dependence on the absorption coefficient of the analyte:

#86369 - $15.00 USD Received 13 Aug 2007; revised 15 Sep 2007; accepted 17 Sep 2007; published 24 Sep 2007

$$\frac{dM_0}{M_0} \cong -\left(\frac{1-x}{1+x}\right)\frac{f}{\alpha_i + f\alpha_s}\, d\alpha_a \cong -L_{eff}^{t}\, d\alpha_a . \tag{4}$$

In the absence of solvent absorption, this effective absorption path length can be expressed as

$$L_{eff}^{t} = \left(\frac{1-x}{1+x}\right)\frac{f}{\alpha_i}. \tag{5}$$

This effective length is defined in the low-analyte-absorption limit, $\alpha_a L_{eff}^{t} << 1$ (or $f\alpha_a << \alpha_i$), which is the condition for Eq. (4) to hold. Note that in the strongly undercoupled or overcoupled limits ($x << 1$ or $x >> 1$) the relative detection sensitivity is determined by the intrinsic loss only. This can be advantageous, since having the tapered fiber in contact with the microresonator tends to produce overcoupling, especially when the system is immersed in a liquid. Thus in the strongly overcoupled case, this method has greater relative sensitivity (here, fractional change in dip depth) than the frequency-shift, mode-width, or ringdown methods, all of whose relative sensitivities are determined by the total loss. Recall that the total loss determines the linewidth and the cavity lifetime, and in the overcoupled limit coupling loss dominates. The relative frequency-shift sensitivity is measured as a fraction of the linewidth, the change in mode width is relative to the full width, and ringdown measures the fractional change in the overall lifetime.

An experimental effective absorption path length L_{eff}^{e} can be found by measuring the dip depth in the absence of analyte (M_0) and in the presence of analyte ($M_0 + \Delta M_0$):

$$L_{eff}^{e} \cong \frac{1}{\alpha_a}\ln\frac{M_0}{M_0 + \Delta M_0}. \tag{6}$$

As with Eq. (4), this holds for small changes in dip depth or $\alpha_a L_{eff}^{e} << 1$. Comparison of experimental and theoretical effective absorption path lengths for detection of atmospheric trace gases shows good agreement [11], as discussed briefly in Section 4.

This method also allows for sensitive detection of an analyte in a strongly absorbing solvent. In Eq. (4), if $f\alpha_s >> \alpha_i$, the effective absorption path length can still be as large as $1/\alpha_s$. In effect, solvent absorption can shift the sensor from one sensitive regime to another – from strongly overcoupled to strongly undercoupled, enabling absolute analyte sensitivity, i.e., actual signal amplitudes, that would be difficult to achieve in single-pass direct absorption through the same effective path length.

3. Broadband operation

In this model a microsphere, with one prism coupler used to excite precessing modes [12], is taken to be analogous to a ring cavity with two identical partially-transmitting mirrors. Here we will concentrate on the transmitted signal (drop power output, enabled by precession and detected by a spectrometer) rather than the reflected signal (throughput). See Fig. 2 below.

First consider single-frequency response. Summing over round trips and arbitrarily taking the second partially-transmitting mirror to be at half the round-trip distance from the input mirror (the final result will not depend on this choice), gives the drop power fraction:

$$D_\delta = \left|\frac{Te^{-\alpha L/4}e^{i\delta/2}}{1 - r^2 e^{-\alpha L/2}e^{i\delta}}\right|^2 = \frac{T^2}{\left(T + \frac{1}{2}\alpha L\right)^2 + 4\sin^2\frac{1}{2}\delta} = D_0\,\frac{\left(\frac{1}{2}\Delta\delta\right)^2}{\left(\frac{1}{2}\Delta\delta\right)^2 + \left(2\sin\frac{1}{2}\delta\right)^2}. \tag{7}$$

In this system the mode width is $\Delta\delta = 2T + \alpha L$ and the resonant drop fraction is D_0.

#86369 - $15.00 USD Received 13 Aug 2007; revised 15 Sep 2007; accepted 17 Sep 2007; published 24 Sep 2007

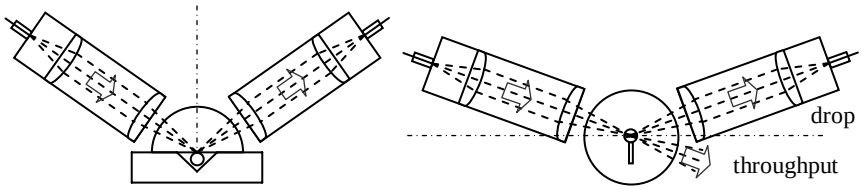

Fig. 2. Hemispherical prism coupling scheme. The microsphere is in a V-groove channel for the solvent and analyte. Left, polar view showing input and output coupling. Right, equatorial view illustrating how precessed light is collected at the drop port.

Now, consider the case where the input is broadband and the drop signal is detected by a spectrometer, which integrates over a frequency interval that we will take to be equal to the FSR (for convenience; again, the final result will not depend on this choice, and the spectrometer resolution interval may be greater than or less than the FSR, as long the conditions noted below are satisfied). Assuming the input power, the reflection and transmission coefficients, and the intrinsic loss all to be independent of frequency over this interval, the integrated drop fraction D_I, the fraction of the incident power in the integration interval that is transmitted out the drop port, is given by

$$D_I = \frac{D_0}{\sqrt{1+\left(\frac{4}{\Delta\delta}\right)^2}} \rightarrow \begin{cases} D_0 = 4T^2/(\Delta\delta)^2 & \text{for } \Delta\delta >> 1 \\ D_0\Delta\delta/4 = T^2/\Delta\delta & \text{for } \Delta\delta << 1 \end{cases}. \tag{8}$$

The spectrometer signal will be proportional to this integrated fraction times the incident power in the detection interval. Note the functional dependence of the detected signal on the linewidth (or total loss) $\Delta\delta = 2T + \alpha L$ in the two limiting cases of large and small linewidth. The first limiting case says that when the linewidth fills the integration interval, the drop fraction equals what would be found by using a single-frequency source tuned to WGM resonance; this holds for either low *Q* or many overlapping modes in the integration interval, so that integration introduces no additional linewidth dependence. The second limiting case is the usual one for well-separated modes, and is the same as that which results from approximating each WGM's narrow transmitted lineshape as a Lorentzian; this holds as long as the integration interval is wide compared to the WGM linewidth.

Let the effective loss coefficient now include, in addition to intrinsic loss, a contribution due to absorption (and scattering) by the analyte filling the evanescent fraction *f* of the WGM: $\alpha = \alpha_i + f\alpha_a$. The effect of the analyte on the resonant (single-frequency) drop signal D_{0a}, when analyte absorption is a small fraction of the total loss, can be written in terms of an approximate effective absorption path length L_{eff} as defined below:

$$D_{0a} = \frac{4T^2}{(2T + \alpha_i L + f\alpha_a L)^2} = \frac{D_0}{\left(1+\frac{1}{2}\alpha_a L_{eff}\right)^2}, \text{ where } L_{eff} = \frac{2fL}{2T+\alpha_i L}. \tag{9}$$

Here, L_{eff} is the effective absorption path length as defined in the low-analyte-absorption limit. However, the last expression for D_{0a} is valid even for large analyte absorption, that is, there are no restrictions on the size of $\alpha_a L_{eff}$ as long as $f\alpha_a L << 1$.

Then, for broadband input, the integrated drop fraction in the presence of analyte, D_{Ia}, will also be given by Equation (9) in the large linewidth limit. For precessing-mode drop-port output collected without being spatially filtered by an aperture [13], this limit applies, for the following reason. The incident focused light (Fig. 2) incorporates a bundle of wavevectors and so excites precessing modes over a range of angles with respect to the

#86369 - $15.00 USD Received 13 Aug 2007; revised 15 Sep 2007; accepted 17 Sep 2007; published 24 Sep 2007

equatorial plane. The round-trip distance depends on this angle in a spheroid, so the precessing modes are frequency-shifted by amounts depending on angle. The result is many modes (not just a range of different angles, but also ranges of different radial orders and different polar orders) that overlap to fill the integration interval, so when the analyte absorption broadens the linewidth and reduces the transmission of each mode, the broadening is not noticed, because the integration interval remains filled. Thus only the decrease in amplitude is observed, just as in the single-frequency resonant case. The overlapping of modes also means that the exact value of the spectrometer resolution interval does not matter. This large-linewidth-limit functional dependence of the integrated drop signal on $\alpha_a L_{eff}$ as given in Eq. (9) has been tested in recent experimental work [14], described briefly below.

4. Discussion and summary

A method for whispering-gallery microcavity-enhanced chemical sensing has been described. Two implementations of this method have been considered in detail. The first involves using a tunable single-frequency laser and observing changes in the depth of the throughput dip caused by absorption by the analyte in the evanescent fraction of a WGM. The relative sensitivity was shown to be determined by the intrinsic loss only, in the cases of strong under- or overcoupling. In these cases, a significant dip can still be observed; for example, $x = 0.05$ or $x = 20$ produce $M_0 = 0.18$. In this example, in the overcoupled case, the total loss is twenty-one times the intrinsic loss, so a ~20× enhancement in relative sensitivity compared to frequency-shift or ringdown methods is obtained. For a wavelength on the order of 1000 nm and typical microresonator values, for example circumference $L \sim 1$ mm, $Q \sim 10^8$, evanescent fraction $f \sim 0.2\%$ (in air) or $f \sim 2\%$ (in water or methanol), effective analyte absorption path lengths on the order of centimeters can be expected, even in strongly absorbing solvents ($\alpha_s \sim 1$ cm^{-1}). Using a cylindrical microresonator with $Q \sim 5\times10^6$ [11], experimental effective path lengths of about 1 cm are found for trace amounts of methane, ethylene, or methyl chloride in air at atmospheric pressure. The dip depth is monitored by locking a WGM to the laser as the laser is scanned over absorption lines for wavelengths around 1.65 μm. Agreement with theoretical effective path lengths is very good.

The second implementation uses a broadband source and spectral detection, using a spectrometer with resolution assumed to be of the order of the resonator's FSR (the FSR is about 200 GHz for a 330-μm diameter microsphere, or 0.2 nm for wavelengths around 550 nm). Precessing modes in a microsphere are employed to give a drop spectrum that is modified by analyte absorption. In this case, the total loss determines the sensitivity, but with prism coupling it is more likely that the system will be in the undercoupled limit. The setup shown in Fig. 2 has been used for the detection of Lissamine Green B dye in pH 5 citrate buffer using a 635-nm LED light source [14]. Effective path lengths of about 1 cm were observed, and the behavior of the drop signal as a function of concentration (hence α_a) was in most cases as predicted by Eq. (9).

Although the agreement so far between experimental results and the theoretical model presented here is encouraging, this analysis has neglected certain effects that might need to be taken into account to do a detailed comparison with future experimental results. One of these is saturation (or reverse saturation) of the absorption in the analyte and perhaps also in the solvent. Another is the effect of the dielectric microresonator's surface on the analyte, through the orientation of molecules that adsorb onto the surface or by the induction of a concentration gradient near the surface.

Acknowledgments

The author acknowledges support from the National Science Foundation (ECS-0329924), the Oklahoma State Regents for Higher Education, and ICx Nomadics, and discussions with Jeromy P. Rezac, Siyka I. Shopova, and Brian N. Strecker. Special thanks go to George Farca for extensive discussions and for providing Fig. 1. Figure 2 was adapted from one generously supplied by Jiangquan Zhang.

#86369 - $15.00 USD Received 13 Aug 2007; revised 15 Sep 2007; accepted 17 Sep 2007; published 24 Sep 2007